



Article

Validating Precise Orbit Determination from Satellite-Borne GPS Data of Haiyang-2D

Jinyun Guo ¹, Guangzhe Wang ¹ , Hengyang Guo ^{1,*} , Mingsen Lin ^{2,3} , Hailong Peng ^{2,3}, Xiaotao Chang ⁴ and Yingming Jiang ⁵

¹ College of Geodesy and Geomatics, Shandong University of Science and Technology, Qingdao 266590, China; guojy@sdust.edu.cn (J.G.); wangguangzhe@sdust.edu.cn (G.W.)

² National Satellite Ocean Application Service, Ministry of Natural Resources, Beijing 100081, China; msln@mail.nsoas.org.cn (M.L.); phl@mail.nsoas.org.cn (H.P.)

³ Key Laboratory of Space Ocean Remote Sensing and Application, Ministry of Natural Resources, Beijing 100081, China

⁴ Land Satellite Remote Sensing Application Center, Ministry of Natural Resources, Beijing 100048, China; cxt@sasmac.cn

⁵ College of Land Resource and Surveying & Mapping Engineering, Shandong Agriculture and Engineering University, Jinan 250100, China; z2021026@sdaeu.edu.cn

* Correspondence: xiaoguo@sdust.edu.cn

Abstract: Haiyang-2D (HY-2D) is the fourth satellite in the marine dynamic satellite series established by China. It was successfully launched on 19 May 2021, marking the era of the 3-satellite network in the marine dynamic environment satellite series of China. The satellite's precise orbit determination (POD) and validations are of great significance for ocean warning and marine altimetry missions. HY-2D is equipped with a laser reflector array (LRA), a satellite-borne Doppler Orbitography and Radiopositioning Integrated by Satellite (DORIS) receiver, and a satellite-borne dual-frequency GPS receiver named HY2 that was independently developed in China. In this paper, the quality of GPS data collected by the HY2 is analyzed based on indicators such as the multipath effect, cycle slips, and data completeness. The results suggest that the receiver can be used in POD missions involving low-Earth-orbit (LEO) satellites. The precise orbits of HY-2D are determined by the reduced-dynamics (RD) method. Apart from POD, validation of orbit accuracy is another important task for LEO POD. Therefore, two external validation methods are proposed, including carrier differential validation using one GPS satellite and inter-satellite differential validation using two GPS satellites. These are based on space-borne carrier-phase data, and the GPS satellites used for POD validation do not participate in orbit determination. The results of SLR range validation cannot illustrate the orbit accuracy in x , y , and z directions particularly, so to make validation results more intuitive, the SLR three-dimensional (3D) validation is proposed based on SLR range validation, and the RMSs in x , y , and z directions are 2.66, 3.32, and 2.69 cm, respectively. The results of SLR 3D validation are the same as those of SLR range validation, which proves that the new external validation method provided by SLR 3D is reliable. The RMSs of carrier differential validation and inter-satellite differential validation are 0.68 and 1.06 cm, respectively. The proposed validation methods are proved to be reliable.

Keywords: HY-2D; reduced-dynamic orbit; carrier differential validation; inter-satellite differential validation; SLR three-dimensional validation



Citation: Guo, J.; Wang, G.; Guo, H.; Lin, M.; Peng, H.; Chang, X.; Jiang, Y. Validating Precise Orbit Determination from Satellite-Borne GPS Data of Haiyang-2D. *Remote Sens.* **2022**, *14*, 2477. <https://doi.org/10.3390/rs14102477>

Academic Editors: Baocheng Zhang and Teng Liu

Received: 4 April 2022

Accepted: 19 May 2022

Published: 21 May 2022

Publisher's Note: MDPI stays neutral with regard to jurisdictional claims in published maps and institutional affiliations.



Copyright: © 2022 by the authors. Licensee MDPI, Basel, Switzerland. This article is an open access article distributed under the terms and conditions of the Creative Commons Attribution (CC BY) license (<https://creativecommons.org/licenses/by/4.0/>).

1. Introduction

Haiyang-2D (HY-2D) is the fourth marine dynamic environment satellite in China. It was successfully launched on 19 May 2021, and the data receiving plan was implemented at the National Satellite Ocean Application Service (NSOAS) on 25 May 2021; the receiving system condition is good, the antenna tracking is normal, and the quality of data is good. The ground receiving system is in the normal task receiving stage. HY-2D, HY-2B, and

HY-2C form a large-scale global marine dynamic environment monitoring system that provides accurate marine dynamic environment information for early warning of marine disasters, sustainable development of marine resources, effective response to global climate change, and marine scientific research [1]. HY-2D adopts an orbit with a regression period of 10 days in the early stage and will change to an orbit with a regression period of 400 days in the later stage. HY-2D is equipped with a laser reflector array (LRA), a satellite-borne Doppler Orbitography and Radiopositioning Integrated by Satellite (DORIS) receiver, and a satellite-borne dual-frequency GPS receiver named HY2 that was independently developed in China.

Due to the high speed and low orbit of low-Earth-orbit (LEO) satellites, observations of LEO satellites by ground tracking stations have the shortcomings of short continuous periods and unsustainable observation [2]. Therefore, one station has fewer observations of SLR and DORIS than that of GPS for LEO satellites. The DORIS system was successfully developed by the National Centre for Space Studies (CNES) and other institutions after nearly 10 years of hard work. It can provide high-precision orbital products in the full arc and is mainly used for precise satellite orbit determination and precise point positioning. DORIS observation has the advantages of a short time frame, all-weather operation, more data, and an even distribution of beacon stations. The satellite-borne GPS data have the characteristics of high accuracy, round-the-clock coverage, and continuity. Since Bertiger et al., (1994) successfully applied the satellite-borne GPS receiver on the TOPEX/Poseidon satellite in 1992 [3], the satellite-borne GPS receiver has been installed on several LEO satellites and become a common technique for LEO satellite orbit determination [4–8].

At present, satellite-borne GPS data are used in precise orbit determination (POD) for Jason [9], SWARM [10], GOCE [11], GRACE [12], and CHAMP, and the GPS POD technique has achieved high-precision orbit results. Accuracy evaluation of orbits is an important task of LEO POD. The commonly used methods are mainly divided into internal validations and external validations. The internal validations mainly include carrier-phase residuals and overlapping orbit validation. The external validation mainly includes comparison with other technical orbit determination results and SLR range validation. The external methods to validate the accuracy of orbits are more conducive to proving the reliability of the results of LEO POD, but the orbits determined by other techniques are sometimes not obtained in time. In addition, the traditional SLR range validation is also constrained to the number of normal points (NP), and shortcomings of the validation method include failure to clearly show the accuracy of orbits in three-dimensions. Deficiencies in these external validation methods prevent the determined accuracy of satellite orbits from being fully validated on time, affecting the use of altimetry data. Formation satellites such as GRACE and GRACE-FO, K-band ranging (KBR) can be used to validate the accuracy of orbits. It is necessary to perform calculations using the orbit determination results to obtain the relative distance and speed between satellites, and then compare them with the KBR data to evaluate the relative orbit accuracy of the satellites [13–15]. Guo et al., (2021) proposed verifying the accuracy of the reduced-dynamics (RD) orbits with onboard DORIS data [16].

The quality of satellite data and the orbit determination strategies are the main factors affecting the POD accuracy [17], and the data quality can also be used to evaluate the performance of the receiver [18]. Hwang et al., (2010) analyzed the data quality of COSMIC and GRACE regarding the multipath effect, ionospheric delay, cycle slip, etc., then evaluated the performance differences of different receivers. The results proved that high-quality observations are the premise of high-precision orbit determination [19]. Gong et al., (2020) proposed the progressive method to determine orbits without estimating the orbit parameters directly, which reduces the error of matrixes and obtains more reliable orbits [20].

The main aim of this paper is to evaluate the performance of the HY2 receiver and the accuracy of the HY-2D RD orbit. Based on the satellite-borne GPS observations, precise ephemeris, and SLR data, three orbit accuracy assessment methods are proposed to evaluate the accuracy of HY-2D RD orbit: carrier differential validation, inter-satellite differential

validation, and SLR three-dimensional (3D) validation. In Section 2, the principle and derivation of three methods of orbit accuracy evaluation are introduced in detail. In Section 3, the data quality of HY-2D collected by the satellite-borne GPS receiver is analyzed with TEQC software regarding the multipath error, cycle slips, and data completeness [21]. The orbit determination strategies are analyzed, and the RD method [22] is used to determine the precise orbits of HY-2D. Carrier-phase residuals are used to evaluate the internal accuracy of POD, and SLR range validation and DORIS validation are used to evaluate the external accuracy. The carrier differential validation, inter-satellite differential validation and SLR 3D validation proposed in this paper are used to evaluate the accuracy of POD, and the reliability of the three methods is verified. Finally, the conclusions are presented.

2. Methods

Assessment of POD accuracy is mainly divided into two categories. The internal validation methods only use some data during POD to check the orbit determination results, such as carrier-phase residuals and overlapping orbit validation. The external validation uses data that were not participated in the orbit determination to check the satellite POD, such as comparing with orbits determined by other techniques and SLR range validation [23]. However, in the absence of other technical orbit determination results, there is only one external method to validate the POD, and the SLR range validation can only show the distance difference and cannot evaluate the POD accuracy in x , y , and z directions.

In this paper, three methods are proposed for the external validation of POD: carrier differential validation, inter-satellite differential validation, and SLR 3D validation. The carrier differential validation uses the carrier-phase data of one GPS satellite and inter-satellite differential validation uses the carrier-phase data of two GPS satellites out of all viewed GPS satellites. Since the selected GPS data were not participated in the orbit determination, they can be regarded as external data to achieve validations of orbits accuracy. The SLR 3D validation can evaluate errors in the x , y , and z directions of the POD, making the results more intuitive. Since none of the data used for the validation has been participating in the orbit determination, these three methods are considered external validation.

The carrier differential validation and inter-satellite differential validation use the GPS carrier-phase data to evaluate POD. Errors caused by the ionospheric delay error, satellite clock bias, receiver clock bias, integer ambiguity, and other factors must be considered if the carrier-phase data are used to validate the accuracy of POD without any processing of difference. While the double-difference method can eliminate the effects of these errors on the carrier, it is a good idea to use the method.

2.1. Carrier Differential Validation Method

The carrier differential validation is a comparison between the distance obtained by using carrier-phase data of adjacent epochs and the distance calculated by coordinates of the GPS satellite and the coordinates of LEO; the orbits of LEO are determined by the RD method. The influence of errors is then eliminated through making difference to obtain the residuals of validation.

HY2 is a dual-frequency receiver, and satellite-borne GPS observations of HY-2D include two frequency carriers (L_1 and L_2) [24–26], so the linear combination method is used to obtain the Ionosphere-Free combination [27] observation as:

$$L_{IF} = \frac{f_1^2}{f_1^2 - f_2^2} L_1 - \frac{f_2^2}{f_1^2 - f_2^2} L_2 \quad (1)$$

where f_1 and f_2 are the frequencies of L_1 and L_2 , respectively; L_1 and L_2 are the carrier-phase observations of the two frequencies; L_{IF} is the Ionosphere-Free combination observation.

The carrier-phase observations corresponding to the two frequencies at epoch t_i are $\varphi_1(t_i)$ and $\varphi_2(t_i)$, respectively, and c is the speed of light. The linear combination (LC) of phase data is [27]:

$$LC_i = 2.54573 \times \varphi_1(t_i) \times \frac{c}{1575.42 \times 1000000} - 1.54573 \times \varphi_2(t_i) \times \frac{c}{1227.6 \times 1000000} \quad (2)$$

where LC_i is the LC observation at epoch t_i , $\varphi_1(t_i)$ and $\varphi_2(t_i)$ are the carrier-phase observations of the two frequencies at epoch t_i .

The difference between the LC observations in the two adjacent epochs is found to obtain the carrier distance difference ΔLC_i :

$$\Delta LC_i = LC_{i+1} - LC_i \quad (3)$$

where LC_i is the LC observation at epoch t_i , and LC_{i+1} is the LC observation at epoch t_{i+1} .

The geometrical distance ρ_i between the HY-2D orbit and the GPS satellite orbit can be calculated as:

$$\rho_i = \sqrt{(x_h - x^s)^2 + (y_h - y^s)^2 + (z_h - z^s)^2} \quad (4)$$

where x_h, y_h, z_h represent the position of HY-2D obtained by POD, x^s, y^s, z^s represent the position of the GPS satellite, and ρ_i is the geometrical distance.

The difference of geometrical distances between two adjacent epochs:

$$\Delta \rho_i = \rho_{i+1} - \rho_i \quad (5)$$

where ρ_i is the geometrical distance at epoch t_i , and ρ_{i+1} is the geometrical distance at epoch t_{i+1} .

The difference between two adjacent epochs is found by using the carrier-phase distance difference and geometrical distance difference, that is, Equation (3) minus Equation (5):

$$\Delta_i = \Delta LC_i - \Delta \rho_i \quad (6)$$

Equation (6) is used to calculate Δ_i and Δ_{i+1} of two adjacent epochs and find the difference again:

$$e_i = \Delta_{i+1} - \Delta_i \quad (7)$$

The residuals can be obtained, and the effect of errors such as satellite clock bias and ambiguity are eliminated.

The core idea of carrier differential validation is that the carrier distance variation and geometrical distance variation between one GPS satellite that is not participating in LEO POD and the LEO satellite at adjacent epochs should be the same in theory. The influence of other errors is eliminated by finding the difference, and the residuals are obtained as a result of the orbital accuracy validation.

2.2. Inter-Satellite Differential Validation Method

The inter-satellite differential validation is a method that uses carrier-phase data of two GPS satellites that are not participating in LEO POD and the precise ephemeris of GPS to calculate the difference between the carrier-phase distances of the adjacent epochs of the two satellites. The orbit determined of LEO and the precise ephemeris of GPS are then used to calculate the geometrical distance between the HY-2D and the GPS satellite to obtain the difference between the carrier-phase distance and the geometrical distance. Finally, the result is differentiated to eliminate the influence of other errors and determine the validation residuals.

Equation (2) is used to obtain Ionosphere-Free combination observations for carrier-phase data, and the carrier distance after eliminating the influence of the ionosphere is LC_i .

The difference between the carrier-phase distance of GPS satellite a and that of GPS satellite b at the same epoch:

$$\Delta LC_i = LC_{ai} - LC_{bi} \quad (8)$$

where LC_{ai} represents the carrier-phase distance between GPS a and HY-2D, and LC_{bi} represents the carrier-phase distance between GPS b and HY-2D; ΔLC_i is the difference of carrier-phase distance between GPS a and GPS b . The geometrical distances ρ_{ai} and ρ_{bi} are calculated using the coordinates of GPS and the coordinates of HY-2D. The difference is found to obtain $\Delta\rho_i$:

$$\Delta\rho_i = \rho_{ai} - \rho_{bi} \quad (9)$$

where ρ_{ai} represents the geometrical distance between GPS a and HY-2D, and ρ_{bi} represents the geometrical distance between GPS b and HY-2D. The carrier-phase distance difference and geometrical distance difference between the two GPS satellites and HY-2D are made differences to obtain the residual e_i :

$$e_i = \Delta LC_i - \Delta\rho_i \quad (10)$$

Since the two GPS satellites that participate in the validations are moving in different directions and at different speeds, the e_i values of the adjacent epochs are differenced to obtain the final residual Δe_i :

$$\Delta e_i = e_{i+1} - e_i \quad (11)$$

The core idea of inter-satellite differential validation is to use the carrier-phase data of two GPS satellites to calculate the relative variations between the two satellites and HY-2D in adjacent epochs and compare them with the relative geometrical distance variations calculated using the coordinates. Therefore, when selecting data for experiments, it is necessary to ensure that two GPS satellites can be observed simultaneously and continuously during this period.

2.3. SLR 3D Validation Method

Since SLR range validation can only determine the residuals of the validation in distance and the results are not very intuitive, we propose an SLR 3D validation method on SLR range validation. SLR 3D validation is a method that uses data about SLR stations and the results of SLR range validation to validate the accuracy of orbits. It uses the coordinates of SLR stations provided by the International Laser Ranging Service (<https://ilrs.gsfc.nasa.gov/>) (accessed on 15 March 2022) (ILRS) and RD orbits of LEO to calculate the geometrical distances from the stations to LEO. Then, make differences between geometrical distances and distances obtained by laser ranging, and the root mean square (RMS) of the results are propagated to three directions according to the law of error propagation, and intuitive results of the validation are obtained.

The latest coordinates of SLR stations (SLRF2014) were downloaded from the ILRS [28], and the coordinates of stations in September 2021 were calculated based on the initial coordinates and the change rate of coordinates provided by SLRF2014. The residuals of distance were obtained according to the principle of laser ranging:

$$\Delta = SLR - \rho \quad (12)$$

where SLR is the laser ranging distance and ρ is the geometrical distance calculated between the SLR station and HY-2D. According to the law of error propagation, the error is transmitted to x , y , and z directions:

$$\delta_{\Delta}^2 = \delta_{SLR}^2 + \left(\frac{\Delta x}{\rho}\right)^2 \times \delta_{x1}^2 + \left(\frac{\Delta y}{\rho}\right)^2 \times \delta_{y1}^2 + \left(\frac{\Delta z}{\rho}\right)^2 \times \delta_{z1}^2 + \left(\frac{\Delta x}{\rho}\right)^2 \times \delta_x^2 + \left(\frac{\Delta y}{\rho}\right)^2 \times \delta_y^2 + \left(\frac{\Delta z}{\rho}\right)^2 \times \delta_z^2 \quad (13)$$

where δ_{Δ} is the RMS of the SLR range validation; δ_{SLR} is the RMS error of the accuracy of range data of the SLR station; Δx , Δy , and Δz are the coordinate differences between the SLR station and the HY-2D satellite in the x , y , and z coordinates during the continuous observation period; δ_{x1} , δ_{y1} , and δ_{z1} represent the accuracy of the coordinates of SLR stations in three directions; δ_x , δ_y , and δ_z are the errors in the results of the validation of orbits in three directions.

The SLR 3D validation method is an improved method based on the SLR range validation method. The new method can express the accuracy of an orbit in the three directions of x , y , and z , making the results more intuitive.

3. Results and Discussion

3.1. Quality Analysis of Satellite-Borne GPS Data

The satellite signals received by the GPS receiver consist of the direct signal and a superimposed signal of reflection; the latter can affect the quality of the observations. The impact on the pseudo-range can reach tens of meters, while the impact on the carrier phase is small, at only a few centimeters. Multipath errors are closely related to antenna characteristics, receiver environments, incidence angle, etc. It is difficult to establish a uniform and accurate model, so the multipath effect is considered one of the most important factors affecting the quality of data [29,30].

Based on the linear combination of pseudo-range observations and carrier-phase observations, multipath errors of L_1 and L_2 frequency can be calculated [31]:

$$MP1 = M_1 - \left(1 + \frac{2}{\alpha - 1}\right)n_1\lambda_1 + \left(\frac{2}{\alpha - 1}\right)n_2\lambda_2 - \left(1 + \frac{2}{\alpha - 1}\right)\varphi_1 + \left(\frac{2}{\alpha - 1}\right)\varphi_2 \quad (14)$$

$$MP2 = M_2 - \left(\frac{2\alpha}{\alpha - 1}\right)n_1\lambda_1 + \left(\frac{2\alpha}{\alpha - 1} - 1\right)n_2\lambda_2 - \left(\frac{2\alpha}{\alpha - 1}\right)\varphi_1 + \left(\frac{2\alpha}{\alpha - 1} - 1\right)\varphi_2 \quad (15)$$

where M_i is the multipath effect of pseudo-range on both frequencies; $\alpha = \frac{f_1^2}{f_2^2}$; n_i and λ_i denote the integer ambiguity of carrier-phase L_i and wavelength of the carrier-phase L_i ; φ_i denotes the multipath noise of L_i band.

The carrier-phase multipath as well as the elevation angle of G03 as observed from HY-2D were calculated and are shown in Figure 1. Figure 1a,c illustrate statistical assessments of MP1 and MP2 and elevation angles, while Figure 1b,d illustrate the exceptional cases of MP1 and MP2 during the period when the GPS satellite was just locked by the satellite-borne GPS receiver at the beginning of the observations.

It can be seen from (a) that MP1 converged rapidly when the satellite elevation angle was greater than 60° . When elevation angles were less than 60° , MP1 fluctuated more; the fluctuations were between -2 and 2 m. During the period in Figure 1b, the satellite elevation angles were all less than 45° , so MP1 fluctuated greatly throughout the period and no convergence occurred. The phenomenon indicated in (b) was a rare occurrence.

At the beginning when the receiver locked GPS and started to collect observations, MP2 maintained a large negative value, and after a short period, it returned to normal. Figure 1c reflects that the change of elevation angle did not have a drastic effect on MP2; when the elevation angle was greater than 40° , MP2 always fluctuated within a small range of about -0.2 to 0.2 m and within -0.5 to 0.5 m overall. During the period in Figure 1d, the satellite elevation angles were all less than 30° , so the MP2 fluctuated more, and the overall fluctuation ranged between -2 and 2 m.

The number of satellites observed can reflect the quality of the data and thus the stability of the receiver. Through the quality analysis of HY-2D satellite-borne GPS data for 7 days from DOY 262 to 268, six or more satellites could be observed 78.7% of the time, and fewer than four satellites were observed only 0.15% of the time. O/slps represents the ratio of the actual number of epochs observed over a period to the number of cycle slips epochs; the more cycle slips occurring, the smaller the O/slps will be. Data completeness represents the ratio of the actual number of epochs observed by the GPS receiver to the

theoretical number of epochs in a period, while in the actual process of data acquisition various factors may lead to missing data. The data utilization rate is the ratio of the actual number of epochs observed by four or more satellites with dual-frequency observations to the theoretical number of epochs observed.

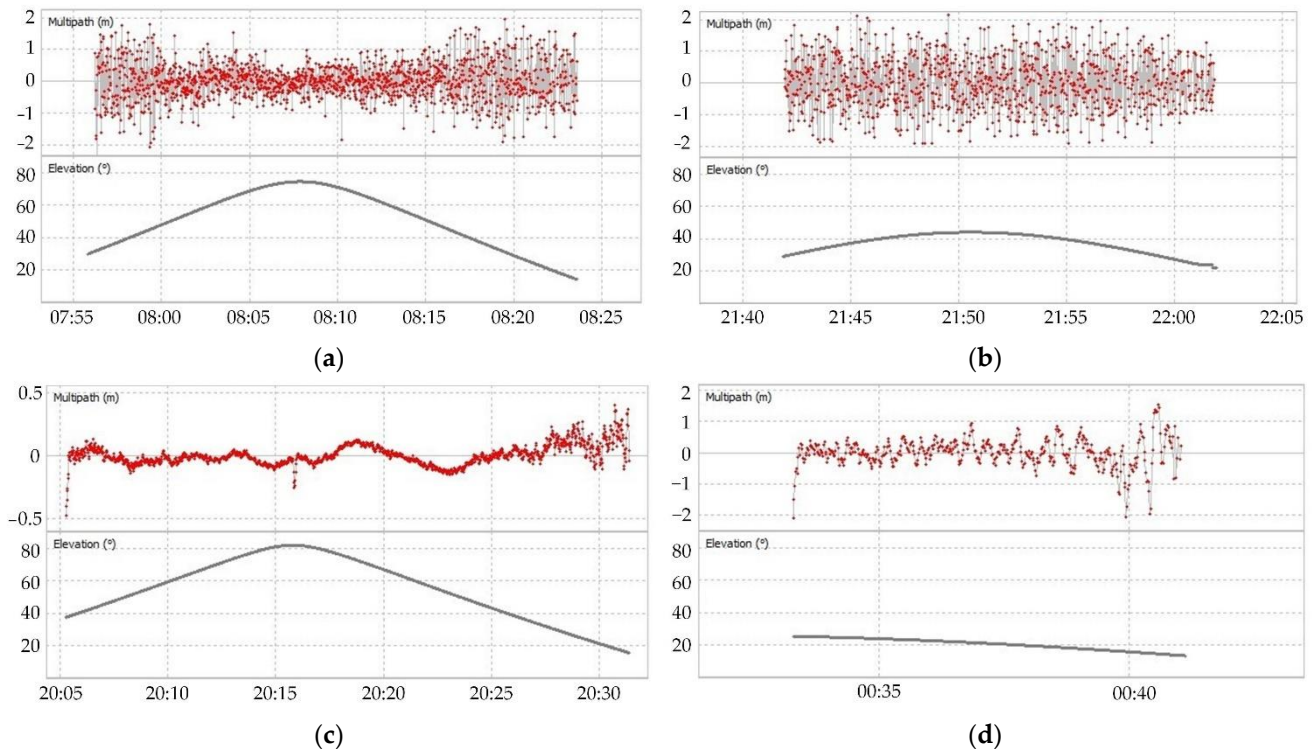


Figure 1. Multipath effects of HY-2D and G03 on DOY 266 in 2021. (a,b) MP1; (c,d) MP2.

The multipath error, cycle slips, and data completeness of the 7 days of satellite-borne GPS data were calculated and tabulated in Table 1. The errors of MP1 and MP2 were 0.35 and 0.23 m, respectively, and MP1 was about 1.5 times that of MP2. The HY-2D observation of DOY 265 was missing in the period from 19:49 to 23:27, resulting in a significantly lower than average data completeness and utilization rate.

Table 1. HY-2D data quality assessment.

DOY	MP1 (m)	MP2 (m)	O/slps	Completeness Rate	Utilization Rate
262	0.39	0.27	45	99.95%	99.33%
263	0.35	0.21	48	99.62%	98.02%
264	0.31	0.22	54	99.95%	98.82%
265	0.33	0.23	53	84.80%	84.43%
266	0.36	0.20	84	99.94%	99.26%
267	0.30	0.22	30	99.95%	98.70%
268	0.40	0.24	42	99.88%	98.68%

3.2. Orbit Determination Strategies and Analysis of Accuracy

HY-2D satellite-borne GPS data are released by NSOAS with a sampling interval of 1 s. The precise ephemeris, precise clock offsets, DCB correction, etc., required for POD are provided by the Centre for Orbit Determination in Europe (CODE). The accuracy validation of orbits is carried out using the SLR data provided by the ILRS and precise ephemeris provided by the International GNSS Service (IGS). Detailed information about the data used in the article is shown in Table 2.

Table 2. Sources of data.

Data	Organization	Address
Satellite-borne GPS data	NSOAS	https://osdds.nsoas.org.cn (accessed on 15 March 2022)
GPS precise ephemeris	CODE	ftp://ftp.aiub.unibe.ch/CODE/2021 (accessed on 15 March 2022)
GPS precise clock bias	CODE	ftp://ftp.aiub.unibe.ch/CODE/2021 (accessed on 15 March 2022)
Earth rotation parameter	CODE	ftp://ftp.aiub.unibe.ch/CODE/2021 (accessed on 15 March 2022)
SLR tracking data	ILRS	https://cddis.nasa.gov/archive/slr/data/npt_crd/hy2d/2021/ (accessed on 15 March 2022)
DORIS data	IDS	ftp://doris.ign.fr/pub/doris/data/h2d/2021 (accessed on 15 March 2022)
SLR station data	ILRS	https://ilrs.gsfc.nasa.gov/archive/slr/products/resource/ (accessed on 15 March 2022)

3.2.1. Orbit Determination Strategies

LEO satellites are mainly affected by conserved and non-conserved forces, and in order to eliminate the influence of these forces on satellite motion, various mechanical models and pseudo-random parameters were added to the RD orbit determination process [32,33]. XGM2019 (120 × 120 orders) was used to eliminate the Earth's gravity; TIDE2000 and FES2004 [34] to eliminate solid and ocean tides [35]; and DE405 to eliminate the effects of multi-body ingress (Sun, Jupiter, Saturn, Uranus, Neptune Venus, etc.) [36]. The strategies used in the POD of HY-2D are shown in Table 3.

Table 3. Reduced-dynamic orbit determination strategy for HY-2D.

Model/Parameters	Description
HY-2D satellite-borne GPS data	Sampling interval 1s
Global Gravity Feld Model	XGM2019 (120 × 120 degree)
N-body	JPL DE405
Relativity	IERS2010XY
Solid-earth tides	TIDE2000
Ocean Tides	FES2004
Elevation cutoff	5°

This study used HY-2D spaceborne GPS data for 7 days from 19 to 24 September 2021 (DOY 262-DOY 268) for POD [37]. Arc lengths of 24 h were selected, and the pulses were estimated every 6 min. The RD orbits were validated using internal and external validation methods. Using observations collected by the HY2 receiver to analyze the accuracy of orbits in internal validation, the carrier-phase residuals were used to assess the accuracy of HY-2D RD orbit in experiments. The external validation methods used data independent of the POD to assess the accuracy of orbits. In addition to the SLR range validation, the proposed three methods including carrier differential validation, inter-satellite differential validation, and SLR 3D validation were also used, and results indicated that these three methods were reliable.

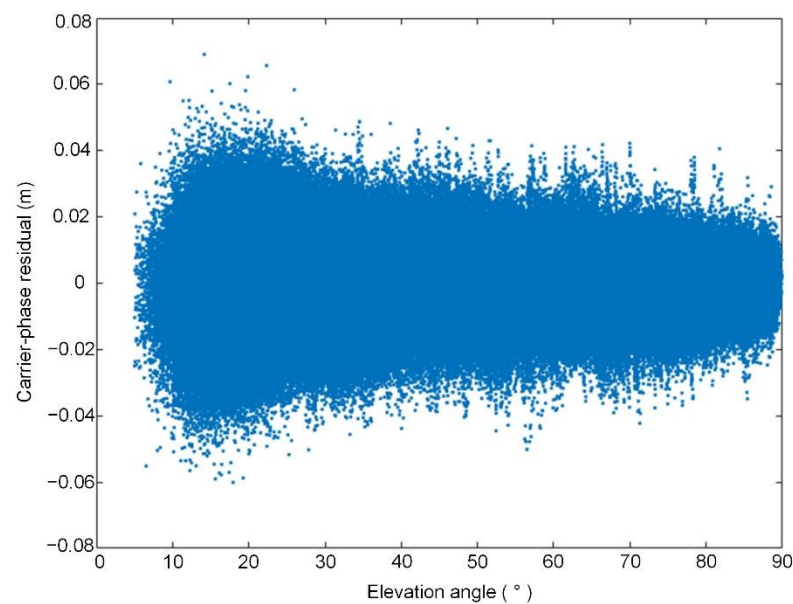
3.2.2. Carrier-Phase Residuals Analysis

The carrier-phase residuals are an important indicator for testing the orbit determination method, reflecting the degree to which observations and the mechanical model are adapted to the actual situation [38]. The quality of the observations, the length of the POD arc, and the parameters to be estimated are all important factors influencing the carrier-phase residuals [39]. The carrier-phase residuals of RD orbits were calculated over 7 days starting from DOY 262 in 2021, and summaries are shown in Table 4.

As shown in Table 4, the carrier-phase residuals fluctuated from −0.0601 to 0.0691 m, with more than 99.4% of the residuals distributed within ±0.025 m, and the fluctuation was relatively gentle. The 7 day RMS values of the carrier-phase residuals fluctuated between 7 and 8.1 mm, and the fluctuation range was only 1.1 mm, which indicated that the strategy and dynamics model we used in POD were reliable and could determine RD orbits with high accuracy. The sequence of carrier-phase residuals depending on the elevation angle is plotted in Figure 2.

Table 4. Statistics of carrier-phase residuals.

DOY	Max (m)	Min (m)	RMS (m)
262	0.0581	−0.0579	0.0076
263	0.0656	−0.0588	0.0078
264	0.0623	−0.0590	0.0079
265	0.0608	−0.0551	0.0079
266	0.0584	−0.0601	0.0070
267	0.0551	−0.0572	0.0080
268	0.0691	−0.0517	0.0081

**Figure 2.** Carrier-phase residuals sequence.

As shown in Figure 2, the RMS of the residuals was 7.8 mm, indicating the high accuracy of the carrier observations of HY-2D. The carrier-phase residuals were large when the elevation angles were less than 20°; the main reason for the phenomenon was that the receiver's ability to capture the signal was poor when the elevation angles were too low, resulting in poor quality of observations. Therefore, in the process of POD, the low-elevation angle data with poor quality could be deleted by setting the cut-off elevation angle. The cut-off elevation angle set in the process of orbit determination in this study was 5°.

3.2.3. SLR Range Validation

SLR range validation is the method of calculating the difference between laser ranging and geometric distance using the coordinates of the GPS satellites and the coordinates of the stations [40]. The ranging accuracy reaches 1 cm, making it one of the most widely used external methods [41]. When POD accuracy is assessed using SLR range validation, ocean tide, solid-earth tide, and polar tide models are used to eliminate the effect of tidal correction, and station velocities provided by ITRF2014 are used to eliminate the effect of plate motion. The tropospheric delay correction, center of mass correction, general relativity correction, and station eccentricity correction are performed on the SLR observations. This article used the coordinates and speeds of stations provided by ILRS in SLRF2014 as a priori values. During the 7 days from DOY 262 to DOY 268 in 2021, a total of 19 stations participated in tracking HY-2D.

During the experiment, a total of 1407 normal point (NP) data from 19 stations were used to validate the orbits of HY-2D. Due to missing observations from HY-2D at DOY 266, the orbit in this period was calculated by Bernese 5.2 internal interpolation, and the results of POD are not accurate. Therefore, the NP data observed during the missing period

needed to be deleted, and a total of 105 NP data were deleted from six stations: 7090, 7810, 7840, 7941, 8834, and 7839. The RMS value of the check and the number of NP data for each station were calculated and are tabulated in Figure 3.

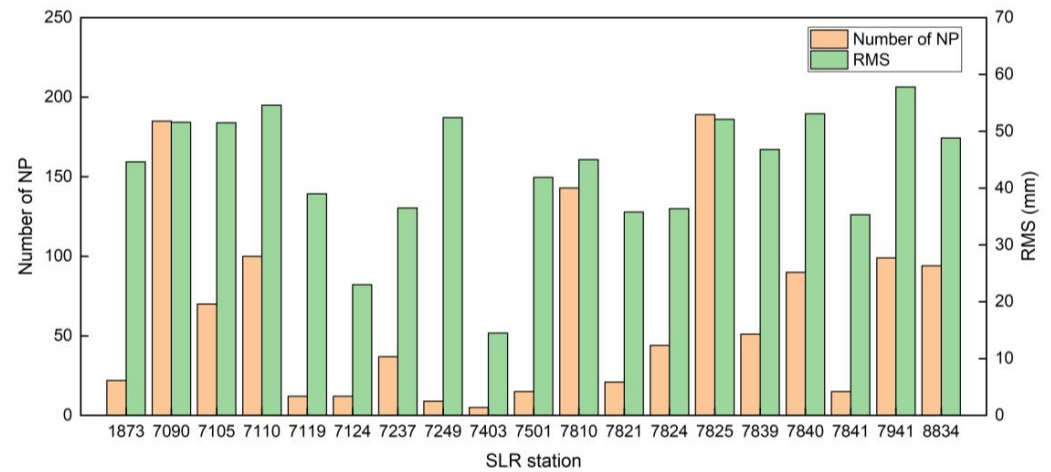


Figure 3. The amount of NP data and the RMS value of the SLR station.

As shown in Figure 3, the 7403 station has the best accuracy of observation with the RMS value of 0.0145 m, but it also has the least number of NP data, with only 7. The worst accurate result of validation is 7941 station, with the RMS value of 0.0578 m and 99 NP data. The 7825 station had the most NP data, with 189, and the RMS value was 0.0521 m. The results of SLR range validation from DOY 262 to DOY 268 in 2021 are summarized in Table 5.

Table 5. Seven day SLR range validation residuals statistics.

DOY	Min (m)	Max (m)	Mean (m)	RMS (m)
262	−0.0968	0.0972	0.0068	0.0485
263	−0.1061	0.0980	0.0100	0.0495
264	−0.1091	0.0930	0.0098	0.0492
265	−0.1097	0.1010	−0.0124	0.0501
266	−0.1059	0.0898	0.0091	0.0450
267	−0.1121	0.0989	0.0032	0.0505
268	−0.1076	0.0972	0.0005	0.0576

When summarizing the SLR range validation residuals of 7 days of RD orbits of HY-2D, the RMS value was 0.0495 m. The results showed that the overall accuracy of the RD orbit of HY-2D obtained by orbit determination was better than 0.05 m.

3.2.4. DORIS Validation

The DORIS orbit check is a method that uses DORIS phase data to validate orbit accuracy through the rate of change in distance. At the time of validation, the elevation cut-off angle was set to 10°, and the DORIS phase data at 10 s intervals were used. Since the time system of the DORIS data was International Atomic Time (TAI) and the RD orbits of HY-2D used GPS time, the first step was to unify the time system. The ionospheric delay effects were removed using a linear combination to obtain the Ionosphere-Free carrier-phase observations LC_i , and the mean distance change rate $d\Delta\phi(t_i)$ was calculated. The mean distance variation rate calculated from the orbits of HY-2D and corrected by various models was $d\rho$. The difference between $d\Delta\phi(t_i)$ and $d\rho$ was calculated to obtain the residuals of DORIS validation [42].

Before using DORIS data to validate, the RD orbit was processed to eliminate the influence of DORIS antenna phase center correction. In order to improve the accuracy of

the validation result, the solid-earth tide, ocean tide and polar tide models were used for tidal correction. The zenith delay was calculated using the Saastamoinen model [43], and then the tropospheric delay was corrected by mapping the signal propagation path using the Niell Mapping Function (NMF) [44]. The results of the DORIS validation for the 7 days of orbits are shown in Table 6.

Table 6. Seven days summary results of DORIS orbit check.

Number of Stations	Min (m/s)	Max (m/s)	RMS (m/s)
42	−0.0585	0.0258	0.0085

The RMS values of the residuals for each station fluctuated between 0.005 and 0.009 m/s. The large errors for the YEMB station and MSPB station were due to a large number of data between 10° and 15° elevation angles; in order to retain more data, the elevation angle of the DORIS validation was set to 10°, because more data at low-elevation angles led to poor inspection results at these stations. Summarizing the statistical results of the 7 days, the RMS residuals value was 0.0085 m/s.

3.3. Accuracy Assessment of RD Orbits by Using the Three New Methods

In addition to the common external methods including SLR range validation and validated by DORIS, the carrier difference validation, inter-satellite differential, and SLR 3D validation proposed in this paper are also used for external validation.

3.3.1. Carrier Differential Validation

The carrier differential validation is a method based on the data on DOY 266 in 2021 for the external validation of orbit, and the period for the receiver to observe the GPS satellite was about 30 min. At the beginning and end of the observations, the elevation angle was less than 40° and the impact of various errors was too large, so data in the middle 1200 epochs with a sample interval of 1 s (20 min) of observations were used for the validation. The data of particular satellites used for the validation does not participate in the POD. The GPS satellite numbers G05, G15, G25, G31 on DOY 266 in 2021 were taken as an example. The results of these satellites are shown in Figure 4.

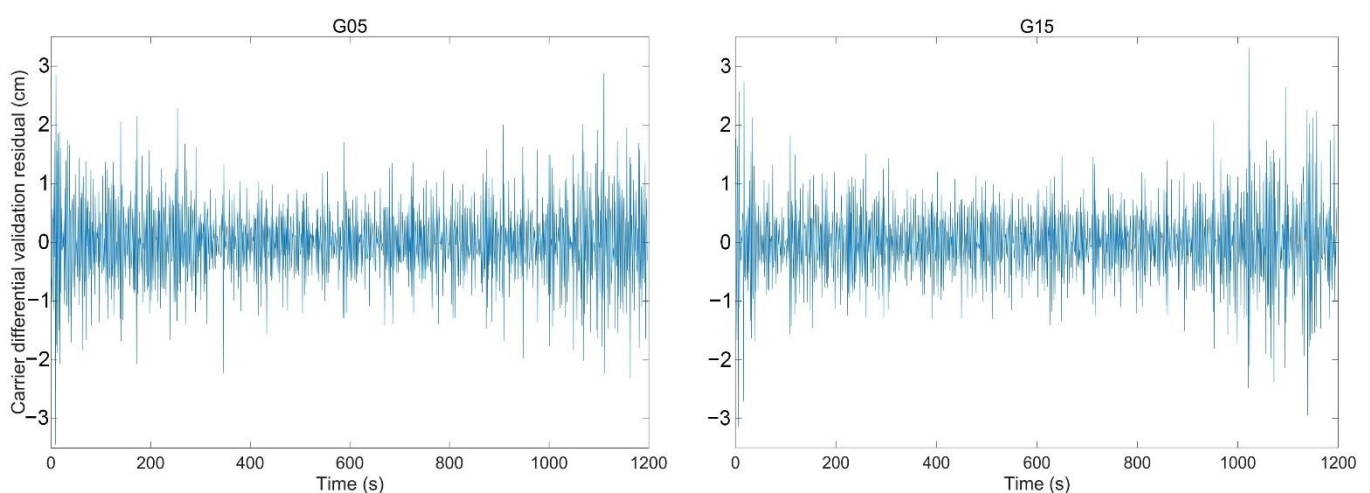


Figure 4. Cont.

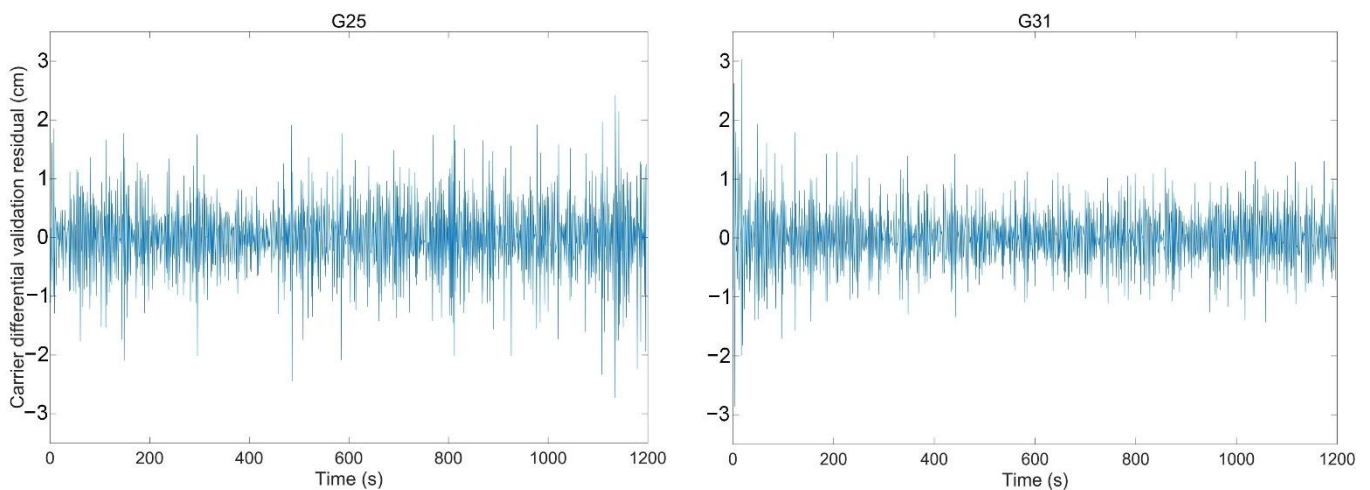


Figure 4. G05, G15, G25, G31 carrier differential validation.

As shown in Figure 4, when using the G05 satellite for the validation, its data were removed from the observations so that they were not used in POD and to ensure that the validation method was an external method. In order to illustrate the reliability of carrier differential validation, experiments were carried out 30 times, with only one set of GPS data removed each time. The results of the validation are shown in Table 7.

Table 7. Carrier differential validation results.

Satellite	Min (m)	Max (m)	RMS (m)
G01	−0.0315	0.0290	0.0070
G02	−0.0337	0.0307	0.0070
G03	−0.0319	0.0364	0.0077
G04	−0.0397	0.0299	0.0076
G05	−0.0343	0.0287	0.0071
G06	−0.0260	0.0222	0.0060
G07	−0.0228	0.0250	0.0064
G08	−0.0251	0.0196	0.0060
G09	−0.0340	0.0261	0.0058
G10	−0.0263	0.0230	0.0069
G12	−0.0251	0.0223	0.0062
G13	−0.0329	0.0424	0.0078
G14	−0.0211	0.0238	0.0063
G15	−0.0314	0.0331	0.0069
G16	−0.0298	0.0315	0.0061
G17	−0.0184	0.0176	0.0054
G18	−0.0318	0.0306	0.0074
G19	−0.0270	0.0274	0.0069
G20	−0.0344	0.0348	0.0090
G21	−0.0345	0.0405	0.0077
G22	−0.0239	0.0307	0.0069
G23	−0.0405	0.0501	0.0087
G24	−0.0230	0.0296	0.0061
G25	−0.0272	0.0242	0.0068
G26	−0.0211	0.0299	0.0065
G27	−0.0241	0.0297	0.0068
G29	−0.0218	0.0235	0.0058
G30	−0.0229	0.0194	0.0056
G31	−0.0286	0.0302	0.0055
G32	−0.0196	0.0200	0.0054
Total	−0.0405	0.0501	0.0068

The results of the G11 and G28 satellites are not listed in the Table 7 because there were no observations of either on DOY 266 in 2021. The RMS value of the residuals for each satellite was better than 0.009 m, and the total RMS value was 0.0068 m. When using each satellite for validation, the fluctuation range of residuals obtained was constant and the mean value was close to 0, indicating that the carrier differential validation method could effectively eliminate the influence of errors on the carrier, so as to obtain reliable accuracy evaluation results.

3.3.2. Inter-satellite Differential Validation

The observations of HY-2D satellite-borne GPS were first processed, and then the data of the satellites involved in the validation were selected according to the distribution of the time series of GPS satellites that were observed. The distribution of GPS satellites observed by the HY2 receiver is shown in Figure 5.

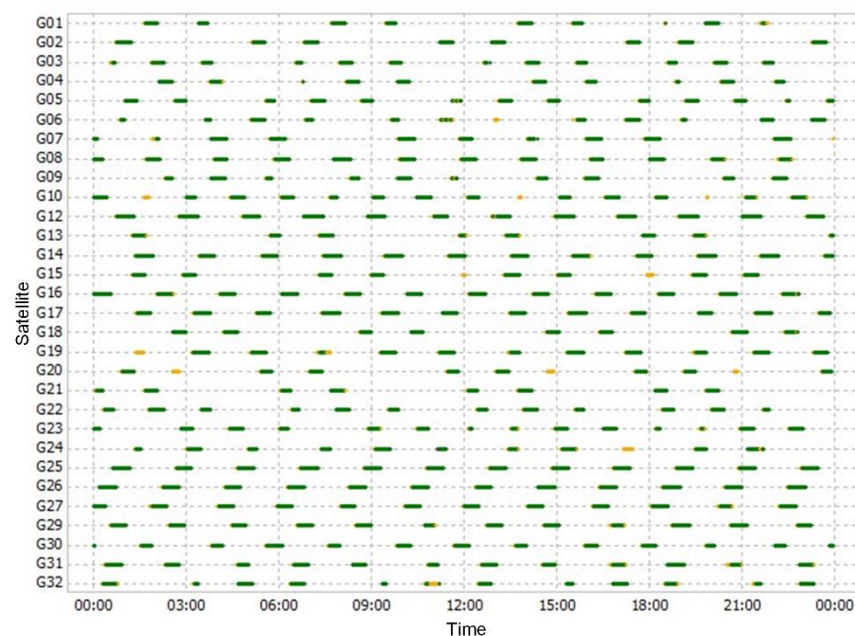


Figure 5. DOY 266 GPS Satellite distribution overview.

As shown in Figure 5, select data of two or more GPS satellites were observed each hour, so one data set was selected each hour for the experiment, and a total of 24 data sets were selected. Due to the short overlap period between the two GPS satellites, the data of 600 epochs with a sampling interval of 1 s (10 min) in the middle of the overlapping period were taken for experiments.

Two data sets of GPS satellites were selected for validation each hour and the data of these two GPS satellites were removed from the observations used in POD. A total of 24 sets of experiments were performed, and, as far as possible, two different satellites were selected for validation to ensure the reliability of the inter-satellite differential validation method. The results are shown in Table 8.

As shown in Table 8, the RMS of the inter-satellite differential validation residuals was better than 1 cm in most periods, with fluctuations in the range of -0.03 to 0.03 m. The total RMS value of residuals on DOY 266 in 2021 was 0.0106 m, and the residuals of each satellite fluctuated in the same range, with fewer fluctuations, so it can be said that inter-satellite differential validation can be used as a reliable external validation method.

Table 8. Inter-satellite differential validation residuals.

Time	Satellite	Max (m)	Min (m)	Mean (m)	RMS (m)
0:00–1:00	G16–G26	0.0288	−0.0231	0.0028	0.0084
1:00–2:00	G01–G21	0.0209	−0.0210	0.0005	0.0072
2:00–3:00	G01–G21	0.0206	−0.0222	−0.0012	0.0075
3:00–4:00	G17–G19	0.0194	−0.0233	0.0001	0.0072
4:00–5:00	G07–G30	0.0404	−0.0393	−0.0007	0.0119
5:00–6:00	G02–G06	0.0325	−0.0327	0.0000	0.0118
6:00–7:00	G07–G08	0.0262	−0.0289	−0.0026	0.0084
7:00–8:00	G13–G15	0.0294	−0.0202	0.0041	0.0097
8:00–9:00	G08–G27	0.0457	−0.0438	−0.0031	0.0119
9:00–10:00	G17–G19	0.0214	−0.0213	−0.0021	0.0074
10:00–11:00	G04–G09	0.0352	−0.0392	−0.0045	0.0121
11:00–12:00	G12–G19	0.0414	−0.0356	−0.0043	0.0190
12:00–13:00	G08–G27	0.0225	−0.0241	0.0013	0.0080
13:00–14:00	G17–G19	0.0450	−0.0515	−0.0023	0.0159
14:00–15:00	G16–G26	0.0260	−0.0238	0.0020	0.0090
15:00–16:00	G12–G15	0.0206	−0.0263	−0.0040	0.0085
16:00–17:00	G09–G30	0.0299	−0.0303	−0.0021	0.0109
17:00–18:00	G02–G06	0.0297	−0.0277	0.0024	0.0117
18:00–19:00	G16–G26	0.0227	−0.0237	0.0010	0.0083
19:00–20:00	G13–G15	0.0251	−0.0242	0.0031	0.0093
20:00–21:00	G16–G26	0.0210	−0.0202	0.0009	0.0084
21:00–22:00	G12–G25	0.0161	−0.0204	−0.0008	0.0075
22:00–23:00	G07–G30	0.0324	−0.0304	0.0006	0.0097
23:00–24:00	G25–G29	0.0348	−0.0486	−0.0034	0.0145
DOY266	Total	0.0457	−0.0515	−0.0005	0.0106

3.3.3. SLR 3D Validation

The results of SLR range validation are relatively single, and the accuracy of the orbit cannot be more intuitively presented. The SLR 3D validation is a method that uses the position and speed of the SLR station and the results of SLR rang validation to obtain errors in the x, y, and z directions according to the law of error propagation.

Stations with more than 50 NP data were selected for the experiment, and a total of nine stations met the experimental requirements. Each selected station provided three consecutive observation periods, and the RMS in the x, y, and z directions were obtained by solving the equations, as shown in Table 9.

Table 9. RMS of SLR 3D validation residuals.

Station	X (m)	Y (m)	Z (m)	3D (m)
7090	0.0257	0.0352	0.0331	0.0547
7105	0.0110	0.0390	0.0364	0.0545
7110	0.0240	0.0372	0.0287	0.0528
7810	0.0250	0.0199	0.0260	0.0412
7825	0.0300	0.0387	0.0150	0.0512
7839	0.0229	0.0379	0.0203	0.0487
7840	0.0265	0.0289	0.0253	0.0467
7941	0.0416	0.0319	0.0338	0.0579
8834	0.0229	0.0242	0.0137	0.0360
Total	0.0266	0.0332	0.0269	0.0503

As shown in Table 9, the errors in three directions of every station were better than 0.042 m, and the 3D RMS was better than 5.8 cm. When combining all stations, the RMS values were 0.0266 m in x-direction, 0.0332 m in y-direction, 0.0269 m in z-direction, and the 3D RMS value was 0.0503 m. The 3D RMS value was close to the result of SLR range

validation, which proved that this method is reliable and can more intuitively evaluate the 3D accuracy of orbits based on the SLR range validation.

4. Conclusions

In this paper, the quality of HY-2D satellite-borne GPS data was analyzed, and the receiver was able to observe six or more navigation satellites more than 78.6% of the time. Compared with the L_2 frequency data, the variation in elevation angle had a greater impact on the L_1 frequency carrier-phase observations. The elevation angles were consistently below 40° for some of the observations, resulting in a large multipath error and severe fluctuations. The multipath effect, data integrity rate, and cycle slips proved that the HY2 receiver independently developed in China had a good performance and stable operation. Three external methods including carrier differential validation, inter-satellite differential validation, and SLR 3D validation were proposed, and the feasibility of these methods was verified based on the RD orbit of HY-2D. The orbits of HY-2D were precisely determined using the RD method; the carrier-phase residual was used as the internal validation method, and the residual RMS value was 0.0078 m. The DORIS validation and SLR range validation were used as the external validation methods with RMS values of 0.0085 m/s and 0.0495 m, respectively. The proposed SLR 3D validation based on the SLR range validation obtained errors in the x, y, and z directions, and the RMS values were 0.0266, 0.0332, and 0.0269 m, respectively. The results were comparable to the accuracy of SLR range validation but more intuitive. The proposed carrier differential validation and inter-satellite differential validation were mainly carried out using satellite carrier-phase data that was not used in POD. One or two GPS satellites were selected from the satellite-borne GPS data for external validation, and the remaining observations of GPS satellites were used for POD. The RMS values of the carrier differential validation and inter-satellite differential validation were 0.0068 and 0.0106 m, respectively. Experimental results demonstrated that the three proposed methods can be used as external validation methods and that they are reliable.

Author Contributions: Conceptualization, writing—original draft preparation, writing—review and editing and methodology, J.G., G.W. and H.G.; software, G.W.; validation, G.W. and H.G.; formal analysis, X.C. and Y.J.; resources, J.G. and Y.J.; data curation, M.L. and H.P.; funding acquisition, J.G. All authors have read and agreed to the published version of the manuscript.

Funding: This research is supported by the National Natural Science Foundation of China (Grant Nos. 42174041 and 41774001), the Autonomous and Controllable Special Project for Surveying and Mapping of China (Grant No. 816-517), and the SDUST Research Fund (Grant No. 2014TDJH101).

Data Availability Statement: Our sincere thanks go to the National Satellite Ocean Application Center for providing satellite-borne GPS data for HY-2D; CODE for providing GPS satellite orbits, clocks and Earth rotation parameters; the ILRS for providing SLR station data and SLR tracking data; and the IDS for providing DORIS data.

Conflicts of Interest: The authors declare no conflict of interest.

References

1. Jiang, X.W.; He, X.Q.; Lin, M.S.; Gong, F.; Ye, X.M.; Pan, D.L. Progresses on ocean satellite remote sensing application in China. *Haiyang Xuebao* **2019**, *41*, 113–124. [[CrossRef](#)]
2. Zhou, C.C.; Zhong, S.M.; Peng, B.B.; Ou, J.K.; Zhang, J.; Chen, R.J. Real-time orbit determination of Low Earth orbit satellite based on RINEX/DORIS 3.0 phase data and spaceborne GPS data. *Adv. Space Res.* **2020**, *66*, 1700–1712. [[CrossRef](#)]
3. Bertiger, W.I.; Bar-Sever, Y.E.; Christensen, E.J.; Davis, E.S.; Guinn, J.R.; Haines, B.J.; Ibanez-Meier, R.W.; Jee, J.R.; Lichten, S.M.; Melbourne, W.G.; et al. GPS precise tracking of TOPEX/POSEIDON: Results and implications. *J. Geophys. Res. Ocean.* **1994**, *99*, 24449–24464. [[CrossRef](#)]
4. Kang, Z.; Tapley, B.; Bettadpur, S.; Ries, J.; Nagel, P. Precise orbit determination for GRACE using accelerometer data. *Adv. Space Res.* **2006**, *38*, 2131–2136. [[CrossRef](#)]
5. Huang, W.; Männel, B.; Sakic, P.; Ge, M.; Schuh, H. Integrated processing of ground- and space-based GPS observations: Improving GPS satellite orbits observed with sparse ground networks. *J. Geod.* **2020**, *94*, 96. [[CrossRef](#)]
6. Prange, L.; Orliac, E.; Dach, R.; Arnold, D.; Beutler, G.; Schaer, S.; Jäggi, A. CODE's Five-System Orbit and Clock Solution—The Challenges of Multi-GNSS Data Analysis. *J. Geod.* **2017**, *91*, 345–360. [[CrossRef](#)]

7. Švehla, D.; Rothacher, M. Kinematic positioning of LEO and GPS satellites and IGS stations on the ground. *Adv. Space Res.* **2005**, *36*, 376–381. [[CrossRef](#)]
8. Hackel, S.; Montenbruck, O.; Steigenberger, P.; Balss, U.; Gisinger, C.; Eineder, M. Model Improvements and Validation of TerraSAR-X Precise Orbit Determination. *J. Geod.* **2017**, *91*, 547–562. [[CrossRef](#)]
9. Lemoine, F.G.; Zelensky, N.P.; Chinn, D.S.; Pavlis, D.E.; Rowlands, B.D.; Beckley, B.D.; Luthcke, S.B.; Willis, P.; Ziebart, M.; Sibthorpe, A.; et al. Towards development of a consistent orbit series for TOPEX, Jason-1, and Jason-2. *Adv. Space Res.* **2010**, *46*, 1513–1540. [[CrossRef](#)]
10. Li, X.X.; Wu, J.Q.; Zhang, K.K.; Li, X.; Xiong, Y.; Zhang, Q. Real-Time Kinematic Precise Orbit Determination for LEO Satellites Using Zero-Differenced Ambiguity Resolution. *Remote Sens.* **2019**, *11*, 2815. [[CrossRef](#)]
11. Bock, H.; Jäggi, A.; Beutler, G.; Meyer, U. GOCE: Precise orbit determination for the entire mission. *J. Geod.* **2014**, *88*, 1047–1060. [[CrossRef](#)]
12. Mao, X.; Visser, P.; Jose, V. Absolute and relative orbit determination for the CHAMP/GRACE constellation. *Adv. Space Res.* **2019**, *63*, 3816–3834. [[CrossRef](#)]
13. Zhou, X.Y.; Jiang, W.P.; Chen, H.; Li, Z.; Liu, X.X. Improving the GRACE Kinematic Precise Orbit Determination through Modified Clock Estimating. *Sensors* **2019**, *19*, 4347. [[CrossRef](#)]
14. Kang, Z.; Bettadpur, S.; Nagel, P.; Save, H.; Poole, S.; Pie, N. GRACE-FO precise orbit determination and gravity recovery. *J. Geod.* **2020**, *94*, 85. [[CrossRef](#)]
15. Jin, B.; Li, Y.Q.; Jiang, K.C.; Li, Z.L.; Chen, S.S. GRACE-FO Antenna Phase Center Modeling and Precise Orbit Determination with Single Receiver Ambiguity Resolution. *Remote Sens.* **2021**, *13*, 4204. [[CrossRef](#)]
16. Guo, H.Y.; Guo, J.Y.; Yang, Z.M.; Wang, G.Z.; Qi, L.H.; Lin, M.S.; Peng, H.L.; Ji, B. On Satellite-Borne GPS Data Quality and Reduced-Dynamic Precise Orbit Determination of HY-2C: A Case of Orbit Validation with Onboard DORIS Data. *Remote Sens.* **2021**, *13*, 4329. [[CrossRef](#)]
17. Kang, Z.; Tapley, B.; Bettadpur, S.; Ries, J.; Nagel, P.; Pastor, R. Precise orbit determination for the GRACE mission using only GPS data. *J. Geod.* **2006**, *80*, 322–331. [[CrossRef](#)]
18. Montenbruck, O.; Kroes, R. In-flight performance analysis of the CHAMP BlackJack GPS receiver. *GPS Solut.* **2003**, *7*, 74–86. [[CrossRef](#)]
19. Hwang, C.; Tseng, T.P.; Lin, T.J.; Švehla, D.; Hugentobler, U.; Chao, B.F. Quality assessment of FORMOSAT-3/COSMIC and GRACE GPS observables: Analysis of multipath, ionospheric delay and phase residual in orbit determination. *GPS Solut.* **2010**, *14*, 121–131. [[CrossRef](#)]
20. Gong, X.W.; Sang, J.Z.; Wang, F.H.; Li, X.X. A More Reliable Orbit Initialization Method for LEO Precise Orbit Determination Using GNSS. *Remote Sens.* **2020**, *12*, 3646. [[CrossRef](#)]
21. Abou, G.M.; Kaloop, M.R.; Rabah, M.M.; Zeidan, Z.M. Improving Precise Point Positioning Convergence Time through TEQC Multipath Linear Combination. *J. Surv. Eng.* **2018**, *144*, 04018002. [[CrossRef](#)]
22. Visser, P.N.A.M.; Ijssel, V.D. Aiming at a 1-cm Orbit for Low Earth Orbiters: Reduced-Dynamic and Kinematic Precise Orbit Determination. *Space Sci. Rev.* **2003**, *108*, 27–36. [[CrossRef](#)]
23. Kong, Q.L.; Guo, J.Y.; Hwang, C.; Gao, F.; Lin, H.; Zhao, C.M. Precise orbit determination and accuracy analysis of HY-2A satellite using DORIS Doppler data. *Acta Geod. Geophys.* **2014**, *49*, 455–470. [[CrossRef](#)]
24. Zhang, B.C.; Hou, P.Y.; Zha, J.P.; Liu, T. Integer-estimable FDMA model as an enabler of GLONASS PPP-RTK. *J. Geod.* **2021**, *95*, 91. [[CrossRef](#)]
25. Zhang, B.C.; Teunissen, P.J.G.; Yuan, Y.B.; Zhang, X.; Li, M. A modified carrier-to-code leveling method for retrieving ionospheric observables and detecting short-term temporal variability of receiver differential code biases. *J. Geod.* **2019**, *93*, 19–28. [[CrossRef](#)]
26. Zhang, B.C.; Ou, J.K.; Yuan, Y.B.; Li, Z.S. Extraction of line-of-sight ionospheric observables from GPS data using precise point positioning. *Sci. China Earth Sci.* **2012**, *55*, 1919–1928. [[CrossRef](#)]
27. Zhao, Q.L.; Wang, G.X.; Liu, Z.Z.; Hu, Z.G.; Dai, Z.Q.; Liu, J.N. Analysis of BeiDou Satellite Measurements with Code Multipath and Geometry-Free Ionosphere-Free Combinations. *Sensors* **2016**, *16*, 123. [[CrossRef](#)]
28. Altamimi, Z.; Rebischung, P.; Laurent, M.; Collilieux, X. ITRF2014: A new release of the International Terrestrial Reference Frame modeling nonlinear station motions. *J. Geophys. Res. Solid Earth* **2016**, *121*, 6109–6131. [[CrossRef](#)]
29. Li, M.; Li, W.W.; Shi, C.; Jiang, K.C.; Guo, X.; Dai, X.L.; Meng, X.G.; Yang, Z.D.; Yang, G.L. Precise orbit determination of the Fengyun-3C satellite using onboard GPS and BDS observations. *J. Geod.* **2017**, *91*, 1313–1327. [[CrossRef](#)]
30. Schreiter, L.; Montenbruck, O.; Zangerl, F.; Siemes, C.; Arnold, D.; Jäggi, A. Bandwidth correction of Swarm GPS carrier phase observations for improved orbit and gravity field determination. *GPS Solut.* **2021**, *25*, 70. [[CrossRef](#)]
31. Estey, L.H.; Meertens, C.M. TEQC: The Multi-Purpose Toolkit for GPS/GLONASS Data. *GPS Solut.* **1999**, *3*, 42–49. [[CrossRef](#)]
32. Zhang, B.B.; Wang, Z.; Zhou, L.; Feng, J.; Qiu, Y.; Li, F. Precise orbit solution for swarm using space-borne GPS data and optimized pseudo-stochastic pulses. *Sensors* **2017**, *17*, 635. [[CrossRef](#)] [[PubMed](#)]
33. Jäggi, A.; Hugentobler, U.; Beutler, G. Pseudo-Stochastic Orbit Modeling Techniques for Low-Earth Orbiters. *J. Geod.* **2006**, *80*, 47–60. [[CrossRef](#)]
34. Lyard, F.; Lefevre, F.; Letellier, T.; Francis, O. Modelling the global ocean tides: Modern insights from FES2004. *Ocean Dyn.* **2006**, *56*, 394–415. [[CrossRef](#)]

35. Petit, G.; Luzum, B. IERS Conventions. *Bur. Int. Des. Poids Mes. Serv. Fr.* **2010**, *36*, 99–118. Available online: <https://iers-conventions.obspm.fr/content/tn36.pdf> (accessed on 15 March 2022).
36. Ivantsov, A.V. Dynamical model of motion for asteroids based on the DE405 theory. *Kinemat. Phys. Celest. Bodies* **2007**, *23*, 65–69. [[CrossRef](#)]
37. Wang, Z.Y.; Li, Z.S.; Wang, L.; Wang, N.B.; Yang, Y.; Li, R.; Zhang, Y.; Liu, A.; Yuan, H.; Hoque, M. Comparison of the real-time precise orbit determination for LEO between kinematic and reduced-dynamic modes. *Measurement* **2022**, *187*, 110224. [[CrossRef](#)]
38. Mao, X.Y.; Arnold, D.; Girardin, V.; Villiger, A.; Jäggi, A. Dynamic GPS-based LEO orbit determination with 1 cm precision using the Bernese GNSS Software. *Adv. Space Res.* **2020**, *67*, 788–805. [[CrossRef](#)]
39. Liu, M.M.; Yuan, Y.B.; Ou, J.K.; Chai, Y.J. Research on Attitude Models and Antenna Phase Center Correction for Jason-3 Satellite Orbit Determination. *Sensors* **2019**, *19*, 2408. [[CrossRef](#)]
40. Wang, Y.C.; Guo, J.Y.; Zhou, M.S.; Jin, X.; Zhao, C.M.; Chang, X.T. Geometric solution method of SLR station coordinate based on multi-LEO satellites. *Chin. J. Geophys.* **2020**, *63*, 4333–4344. [[CrossRef](#)]
41. Guo, J.Y.; Wang, Y.C.; Shen, Y.; Liu, X.; Sun, Y.; Kong, Q.L. Estimation of SLR Station Coordinates by Means of SLR Measurements to Kinematic Orbit of LEO satellites. *Earth Planets Space* **2018**, *70*, 201. [[CrossRef](#)]
42. Kong, Q.; Guo, J.; Gao, F.; Han, L. Performance Evaluation of Three Atmospheric Density Models on HY-2A Precise Orbit Determination Using DORIS Range-Rate Data. *J. Test. Eval.* **2019**, *47*, 2150–2166. [[CrossRef](#)]
43. Feng, P.; Li, F.; Yan, J.G.; Zhang, F.Z.; Barriot, J.P. Assessment of the Accuracy of the Saastamoinen Model and VMF1/VMF3 Mapping Functions with Respect to Ray-Tracing from Radiosonde Data in the Framework of GNSS Meteorology. *Remote Sens.* **2020**, *12*, 3337. [[CrossRef](#)]
44. Niell, A.E. Global mapping functions for the atmosphere delay at radio wavelengths. *J. Geophys. Res. Solid Earth* **1996**, *101*, 3227–3246. [[CrossRef](#)]